

pubs.acs.org/JACS Article

Mechanistic Insights about Electrochemical Proton-Coupled Electron Transfer Derived from a Vibrational Probe

Sohini Sarkar, Anwesha Maitra, William R. Lake, Robert E. Warburton, Sharon Hammes-Schiffer, and Jahan M. Dawlaty*



Cite This: J. Am. Chem. Soc. 2021, 143, 8381–8390



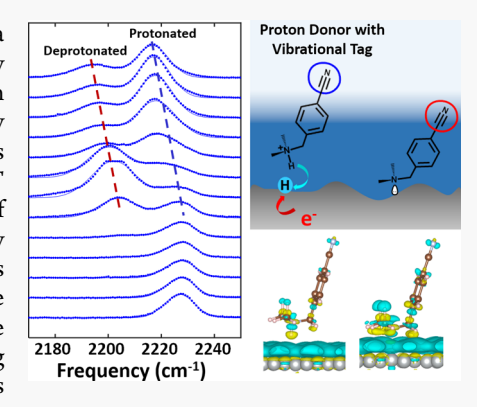
ACCESS

Metrics & More

Article Recommendations

Supporting Information

ABSTRACT: Proton-coupled electron transfer (PCET) is a fundamental step in a wide range of electrochemical processes, including those of interest in energy conversion and storage. Despite its importance, several mechanistic details of such reactions remain unclear. Here, we have combined a proton donor (tertiary ammonium) with a vibrational Stark-shift probe (benzonitrile), to track the process from the entry of the reactants into the electrical double layer (EDL), to the PCET reaction associated with proton donation to the electrode, and the formation of products. We have used *operando* vibrational spectroscopy and periodic density functional theory under electrochemical bias to assign the reactant and product peaks and their Stark shifts. We have identified three main stages for the progress of the PCET reaction as a function of applied potential. First, we have determined the potential necessary for desolvation of the reactants and their entry into the polarizing environment of the EDL. Second, we have observed the appearance of product peaks prior to the onset of steady state electrochemical current, indicating formation of a



stationary population of products that does not turn over. Finally, more negative of the onset potential, the electrode attracts additional reactants, displacing the stationary products and enabling steady state current. This work shows that the integration of a vibrational Stark-shift probe with a proton donor provides critical insight into the interplay between interfacial electrostatics and heterogeneous chemical reactions. Such insights cannot be obtained from electrochemical measurements alone.

■ INTRODUCTION

Reaction of a proton and an electron is one of the most elementary chemical processes. At the electrode surface, this reaction produces an adsorbed hydrogen atom and is called the Volmer reaction, which is the precursor to electrochemical hydrogen evolution. Beyond the Volmer reaction, proton-coupled electron transfer (PCET) is also an elementary step for a variety of electrocatalytic reactions, including water oxidation, CO₂ reduction, and alcohol oxidation in fuel cells. Therefore, understanding the transfer of a proton across the electrical double layer (EDL) and its discharge at an electrode surface is of both fundamental and practical importance.

Although proton discharge from water or $\rm H_3O^+$ is significant and prevalent for many electrocatalytic reactions, the complex hydrogen bonding network in an aqueous environment makes direct spectroscopic characterization of the Volmer reaction challenging. Using a nonaqueous proton donor that mitigates these hydrogen bonding effects can help elucidate properties of the interfacial environment that are relevant to catalysis. Organic ammonium salts in nonaqueous solvents have been used for this purpose 12 and have revealed the importance of nuclear quantum effects in interfacial PCET reactions. 12,13 However, revealing the electrostatic environments that are

experienced by the proton donor in the EDL remains challenging even in nonaqueous solutions. A greater understanding of the electrostatic profile and proton transport across the EDL is critical for the rational control of interfacial electrochemical reactions.

Mechanistic understanding of interfacial PCET is often derived from current—voltage measurements. 3,12,14 While such techniques can be quite powerful, spectroscopic measurements can provide additional mechanistic details of electrochemical reactions. 15 *Operando* spectroscopy, in particular, can aid in the detection of chemical or physical changes near the electrode prior to the onset potential; such insights cannot be obtained from current—voltage relationships alone. 16–18 For example, electrochemical impedance spectroscopy is sensitive to capacitance but averages the behavior over the entire double layer and is not sensitive to the molecular details near the electrode.

Received: February 19, 2021 Published: May 27, 2021





Vibrational spectroscopy can be a useful tool to elucidate the electrostatic environment of the electrochemical interface by using electrolyte molecules as vibrational probes of the local electric field. The particular, benzonitriles are vibrational Stark-shift probes wherein the nitrile vibrational frequency is modified by changes in the electric field experienced by the molecule. Benzonitriles have been used as probes of electrostatics and hydrogen bonding within enzyme cavities. The details of the structure and polarization of a range of interfacial environments. We have used benzonitrile probes to measure the interfacial dielectric solvation reaction fields, the interfacial fields in the presence of aqueous electrolytes and applied potential, fields in the presence of surfactants, fields and hydrogen bonding in the presence of ionic liquid solutions.

Our recent computational work⁴⁰ illustrated the variation of the electrostatic potential on a submolecular length scale across a benzonitrile vibrational probe attached to an electrode. This computational work showed that the nitrile probe vibrational frequency reports changes in the electronic structure of the molecule arising from the electrostatic environment. More specifically, the polarizable benzene ring of the benzonitrile contributes to the sensitivity of the nitrile stretch to the applied potential.

To further understand the Volmer reaction in the context of the structure and dynamics of the interface, we designed an experiment in which a tertiary amine proton donor is tagged with a benzonitrile vibrational Stark-shift probe. The proton donor, 4-[(dimethylammonium)methyl] benzonitrile (abbreviated here as MAMBN-H⁺), is shown in Figure 1. The

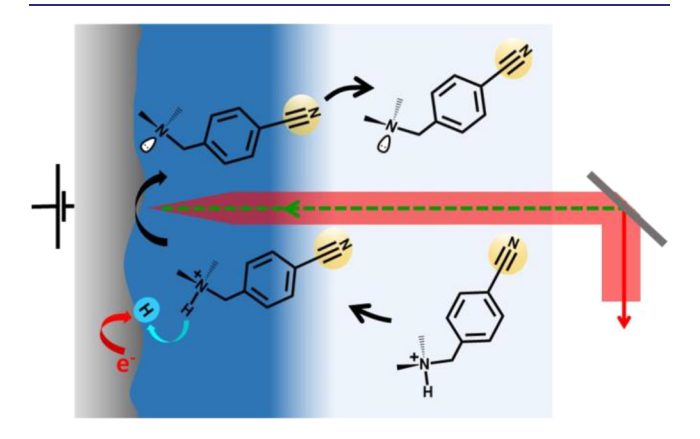


Figure 1. Schematic of the PCET reaction studied using surface enhanced Raman spectroscopy. The tertiary ammonium proton donor with a benzonitrile vibrational tag enters the electric double layer and discharges its proton to the electrode, yielding the amine form. The nitrile probe stretch frequency reports on the details of this process, including the entry of reactants into the EDL, the electric field within the EDL, and adsorption of the products to the surface.

benzonitrile tag is crucial because the protonated reactant (MAMBN-H⁺) and deprotonated product (MAMBN) forms have distinct nitrile vibrational frequencies, providing a spectroscopic signal that reports on the protonation state of the donor. Moreover, the benzonitrile groups of both MAMBN-H⁺ and MAMBN molecules can Stark shift if they reside within the polarizing environment of the EDL. Therefore, changes in the nitrile stretching frequency can provide spectroscopic evidence about the presence of reactants

and products as a function of applied potential, in addition to whether these molecules reside within or outside of the EDL. Installation of a well-defined vibrational probe on the reactant, rather than covalently bound to the surface, reveals crucial electrochemical phenomena that would not be detectable by electrochemical measurements alone or by direct spectroscopy of the mode involved in proton transfer.

Our aim is to describe changes in the interfacial distribution of reactants and products in the EDL with applied potential during the Volmer reaction, including the effects of solvation and interfacial field on MAMBN-H⁺ proton donors and orientation of reactants and products relative to the electrode surface. These insights are relevant to broader fundamental electrochemical challenges such as understanding the desolvation threshold for ionic species, the electrostatics of the interface, and electrode processes prior to the current onset. Moreover, this fundamental knowledge has implications to other fields. For example, ion intercalation in battery electrodes is impeded by desolvation energy, modification of the EDL by surfactants can suppress hydrogen evolution, 22,43 and electrosorption of molecules prior to the thermodynamic onset is relevant to underpotential deposition phenomena.

In this work, we use operando surface enhanced Raman spectroscopy (SERS) to measure the nitrile stretch frequency as a function of potential. These measurements are augmented by computational modeling to describe the protonated ammonium (reactant, MAMBN-H+) and the deprotonated amine (product, MAMBN) near a charged Ag electrode in dielectric continuum solvent. A schematic representation of the process studied herein is shown in Figure 1. Using insights from experimental measurements and theoretical computations, we report three major findings. First, we report the desolvation threshold potential for the proton donor and its entry into the EDL. Second, we identify the appearance of products prior to the onset of steady state electrochemical current, indicating that the reaction can start below the onset for steady state current and yield a static population of products that cannot turn over continuously. Finally, we find that the product remains within the EDL after it is produced and continues to exhibit a Stark shift. The relevance of each finding to the broader range of electrochemical problems will also be discussed.

■ EXPERIMENTAL METHODS

To prepare the ammonium salt, concentrated HCl was added to 4-(dimethylaminomethyl)benzonitrile (MAMBN) obtained from Combi-Blocks. This resulted in formation of a white precipitate of protonated form of 4-(dimethylammonium methyl)benzonitrile (MAMBN-H⁺) which was air-dried. The electrolyte comprised of 100 mM of the reactant and 300 mM of tetrabutylammonium hexafluorophosphate (Sigma-Aldrich) dissolved in DMSO, which is the ideal choice for solvent as it can dissolve both the reactant and the product. Tetrabutylammonium hexafluorophosphate was used as supporting electrolyte. Silver foils of 0.1 mm thickness and 99.9% purity (Sigma-Aldrich) were etched electrochemically and used as the working electrode. Electrochemically etched silver was used as the working electrode because it is an ideal substrate for surface enhanced Raman spectroscopy (SERS).⁴⁶ The reference electrode was Ag/AgCl (Gamry), and a Pt wire was used as the counter electrode. A Gamry Reference 3000 potentiostat was used for step scan voltametry. An etched Ag electrode, a reference electrode, and a Pt wire were placed inside a 3 mL quartz cuvette. A laser source from Ocean Optics Inc. emitting 532 nm was used to excite the SERS active Ag substrates. A Raman probe from InPhotonics held in longitudinal alignment was used to excite and collect backscattered Raman signals from the

samples. The Raman signals were sent to a spectrometer (HORIBA iHR320) with 1800 g/mm gratings with a CCD camera (Syncerity) for spectral analysis. SERS spectra were collected as a function of applied potential. Applied potential was scanned from 0 V to -1.2 V relative to Ag/AgCl reference electrode. Since all experiments were performed in the reductive range of potentials (0 to -1.2 V vs Ag/AgCl), formation of oxide on silver is not expected. After application of each potential step, a transient capacitive current was observed. This transient current was allowed to decay prior to acquiring SERS spectra under steady state electrode condition. At each potential, three SERS spectra were collected with 30 s integration times. The nitrile stretch frequencies were retrieved by fitting the nitrile peaks to Gaussian line shapes using the MATLAB fitting toolbox.

■ COMPUTATIONAL METHODS

We performed periodic density functional theory (DFT) calculations with the dispersion-corrected PBE-D3 functional in Quantum ESPRESSO. ^{47–49} Additional calculations were performed using the PBE⁵⁰ functional, which demonstrated similar trends. Solvent effects were described using a dielectric continuum model via the Environ patch in Quantum ESPRESSO. ⁵¹ In this approach, a modified Poisson equation is solved self-consistently with the Kohn–Sham equations to determine solvation contributions to the total energy. A dielectric constant of 47 was used to model DMSO. ⁵² The electrode potential was modified by varying the number of electrons in the system, which is compensated by a homogeneous background charge. The potential was determined according to previously described methods. ^{14,40,53,54}

Four-layer Ag(111), (100), or (322) surface slabs were employed as models for the Ag electrode. The nitrile stretching frequencies were calculated using a grid-based approach that includes anharmonicity. ⁴⁰ In this implementation, the grid for the surface—molecule system was generated along the approximate normal mode vector corresponding to the nitrile stretch. A one-dimensional potential energy curve was obtained by performing single-point energy calculations at regular intervals along this grid. Subsequently, the Fourier grid Hamiltonian method was used to solve the one-dimensional Schrödinger equation for the nitrile stretch mode represented by this potential, and the nitrile stretch frequency was obtained from the difference between the lowest two vibrational energy levels. For each geometry studied, this method was repeated at different electrode potentials to investigate the vibrational Stark effect. Additional computational details are provided in the Supporting Information (SI).

■ RESULTS AND DISCUSSION

We first describe the nitrile vibrational frequencies of the protonated (MAMBN-H+, reactant) and deprotonated (MAMBN, product) forms of the proton donor. The spectra of neat MAMBN-H+ (solid) and neat MAMBN (liquid) are shown in Figure 2a. The nitrile stretch of MAMBN-H⁺ is blueshifted significantly compared to that of MAMBN. This shift is expected and consistent with previous observations of Stark shift of benzonitrile self-assembled monolayers. 19,35,37,55 A positive charge at the terminal amine produces an electric field at the nitrile similar to that produced by an oxidizing potential, resulting in a blue shift of the nitrile stretch frequency as reported previously.³⁷ Upon dissolving the molecules in DMSO, the nitrile frequencies of both MAMBN-H+ and MAMBN experience red shifts (Figure 2b), which is the expected solvatochromic shift in a high dielectric constant medium.³⁴ It is also seen that MAMBN-H+ experiences a much larger red shift compared to MAMBN, indicating that the positive charge of the ammonium is heavily screened by the solvent. Figure 2c shows the nitrile stretch frequencies of MAMBN-H+ and MAMBN in the presence of a silver electrode at open circuit potential. Both reactants and products experience a red shift with respect to their dissolved forms in

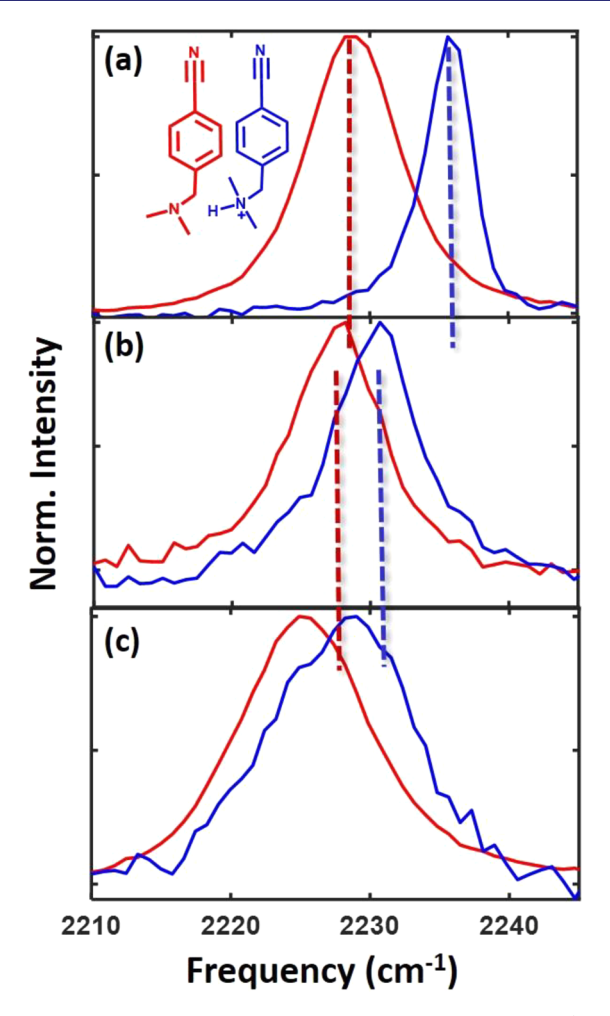


Figure 2. Nitrile stretch spectra of the reactant MAMBN-H⁺ (blue) and the product MAMBN (red) (a) in pure form, (b) dissolved in DMSO, and (c) in the presence of Ag electrode at open circuit potential. The nitrile stretch peak of the product is always red-shifted compared to that of the reactant.

the absence of the Ag electrode. This likely arises due to the participation of the metal in the solvation environment of the molecule, consistent with our previous work on the dielectric solvation near a metal interface.³⁴

Calculations of the nitrile frequencies are qualitatively consistent with the above observations in that they show a blue shift from the product to the reactant and a red shift of both peaks upon solvation (Table S1). These trends were observed with both plane wave and localized Gaussian basis sets using four different functionals. This consistency between the theoretical calculations and the experimental data suggests that the level of theory used in the DFT calculations is appropriate to capture key trends in the nitrile vibrational frequencies. To summarize, the data in Figure 2 show that the protonated MAMBN-H⁺ is always blue-shifted relative to the deprotonated MAMBN and that both are subject to solvatochromic red shifts in the bulk and near the electrode. These spectra serve as a baseline for interpreting the spectroelectrochemical data, which is discussed next.

Figure 3 shows the spectral evolution of the nitrile stretch region as a function of applied potential during the forward (Figure 3a) and reverse (Figure 3c) scans. Figure 3b shows the applied potential and the steady state electrochemical current.

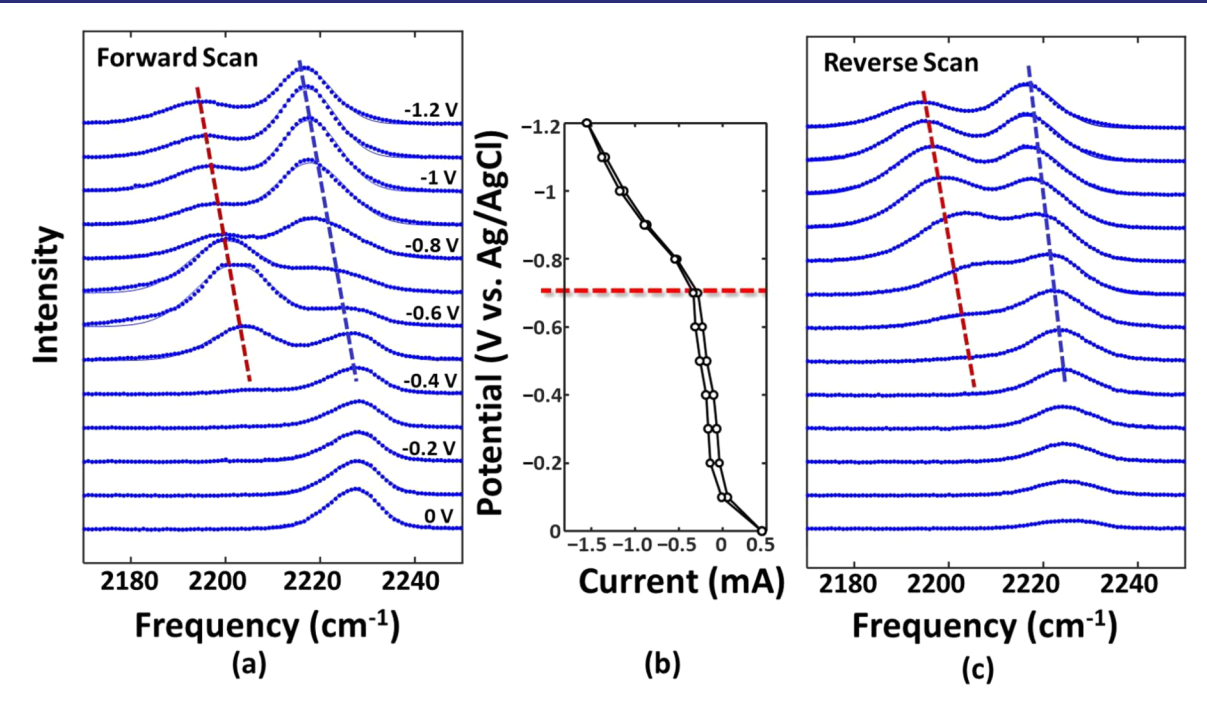


Figure 3. Potential-dependent evolution of the nitrile stretch spectra during the (a) forward and (c) reverse scans. (b) Steady state current versus potential, where the horizontal dotted line at -0.7 V indicates the onset potential for steady state current. The vertical offset of the spectra in panels (a) and (c) is chosen such that each spectrum is aligned with their corresponding potential value in (b). The blue and red dashed lines in (a) and (c) correspond to the Stark shifts attributed to MAMBN-H⁺ and MAMBN, respectively. In the forward scan, initially only the nitrile peak corresponding to the reactant MAMBN-H⁺ is present. It does not undergo a Stark shift, indicating that the reactants are outside the EDL and are not polarized by the electrode. At -0.4 V, a second peak around 2200 cm⁻¹ corresponding to the product MAMBN begins to appear, indicating entry of the reactants into the EDL and formation of products at a potential below the onset of steady state current. Both peaks undergo Stark shifts to lower frequencies with more negative potential, indicating that they arise from species within the EDL because they respond to the polarization exerted by the electrode. The reverse scan shows that the reaction is reversible. Frequency shifts as a function of potential are shown in Figure 4.

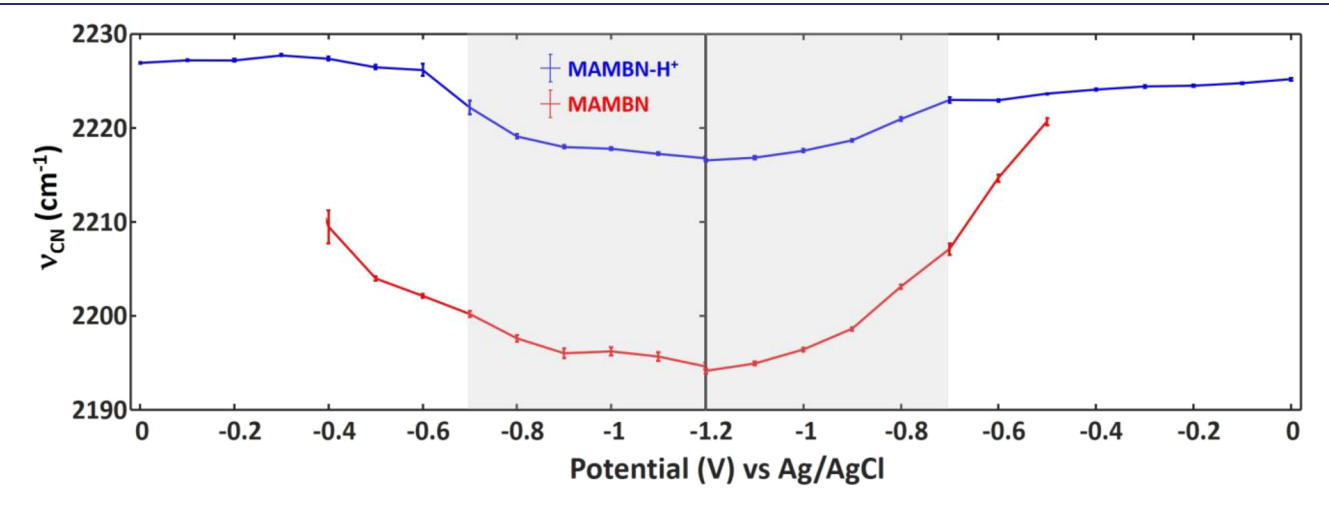


Figure 4. Nitrile frequency of the reactant MAMBN- H^+ (shown in blue) and product MAMBN (shown in red) as a function of applied potential during forward and reverse scans. The gray shaded area represents the region where a steady electrochemical current is measured.

The onset of electrochemical current is near -0.7 V vs Ag/AgCl and is in close agreement with the triethylammonium systems in previous studies. ¹² The frequencies associated with the centers of the dominant two peaks are shown in Figure 4.

Below we will use Figures 3 and 4, along with input from computational work, to describe the desolvation of MAMBN-H⁺, its entry into the EDL, and its eventual conversion into MAMBN following interfacial PCET. To guide the analysis, we discuss the characteristic processes in three distinct potential ranges.

Reactants Outside the Double Layer (0 to -0.4 V). For the most oxidizing potentials in Figure 3 (0 to -0.4 V vs Ag/AgCl), only a single peak is observed, corresponding to the reactant MAMBN-H⁺. Previous work by us and others has shown that self-assembled monolayers of covalently bound benzonitrile are within the electrostatic influence of the electrode and exhibit a significant Stark shift in this potential range. ^{37,55} In the present work, however, this peak shows no Stark shift, indicating that the molecules do not experience the polarizing influence of the electrode in this potential range. Therefore, we propose that the non-Stark shifting peaks in this

potential range arise from MAMBN-H⁺ molecules that are outside the EDL, fully solvated, and shielded from the polarizing influence of the electrode. Note that SERS can detect molecules outside of the EDL because the penetration depth of the SERS technique into the solution is several nanometers, ⁵⁶ while the characteristic thickness of the EDL based on a continuum approximation for DMSO is ~4–8 Å. ^{40,57} This observation further highlights the utility of the Stark reporter, where even its lack of frequency shift is informative and can report on the location of the molecules relative to the EDL.

Entry into the Double Layer and the Initial Reaction (-0.4 to -0.7 V). At potentials more negative than -0.4 V, the nitrile frequency of the reactant MAMBN-H⁺ Stark shifts to lower values (Figures 3a and 4). We propose that at this potential the reactant MAMBN-H⁺ molecules partially shed their bulk solvation shell and enter the EDL, where they experience the polarizing influence of the electrode. Thus, -0.4 V marks the desolvation potential for the protonated form in DMSO. The desolvation threshold of ions near a surface is critically important to many electrochemical processes. A prime example is desolvation of ions in batteries prior to intercalation, where the cost of desolvation is especially high for multivalent ions. 41,58 Our observation of the desolvation threshold using a vibrational reporter could be applicable to such problems.

Since the entry and exit of the reactants and products into and out of the EDL is central to our study, we will briefly highlight the definitions and approximations that go into this understanding. The EDL is the ionic structure near an electrode that forms in response to the applied potential, which, in turn, screens the applied potential. Within the EDL, the electrostatic potential decays with distance from the electrode surface, ⁵⁷ and the resulting electric field can polarize molecules such as Stark-shift probes used in this work. As mentioned above, the Stark response of the benzonitrile probe is influenced by the polarizability of the entire benzene ring conjugated to the nitrile. ³⁶

For our experiments, the characteristic length of the EDL $(\sim 4-8 \text{ Å})$ is comparable to the size of the molecule $(\sim 10 \text{ Å})$. Furthermore, when the probe is oriented with the nitrile pointing away from the electrode and the ammonium end toward the electrode (i.e., prior to the onset of the Volmer reaction, Figure 1), the nitrile bond will reside far from the most polarizing region. Nonetheless, we will demonstrate that the effect of the field will be communicated to that bond via the polarization of the benzene ring.

At -0.4 V, a new peak around 2200 cm⁻¹ appears and is redshifted compared to the reactant peak. We assign this peak to the deprotonated product MAMBN based on experimental and computational evidence, as explained below. The first piece of evidence for assigning this peak to MAMBN is that this peak continues to exist at more negative potentials, where equilibrium favors the products of the reactants. Second, the frequency is red-shifted relative to the reactants, as expected based on the discussion above (Figure 2 and Table S1). However, the red shift is much larger (20 cm⁻¹) than in the bulk solution (~4 cm⁻¹). This difference indicates that, upon formation, the product is closely interacting with the silver electrode surface, potentially chemisorbing through the lone pair of the amine nitrogen, as discussed further below.

We investigated the interactions between the electrode and MAMBN/MAMBN-H⁺ with computational methods. To

account for the polycrystalline Ag electrode used in the experimental portion of this work, we considered several different surface models. In particular, DFT calculations of MAMBN and MAMBN-H⁺ were carried out near three different Ag surfaces. Figure 5 shows optimized geometries of

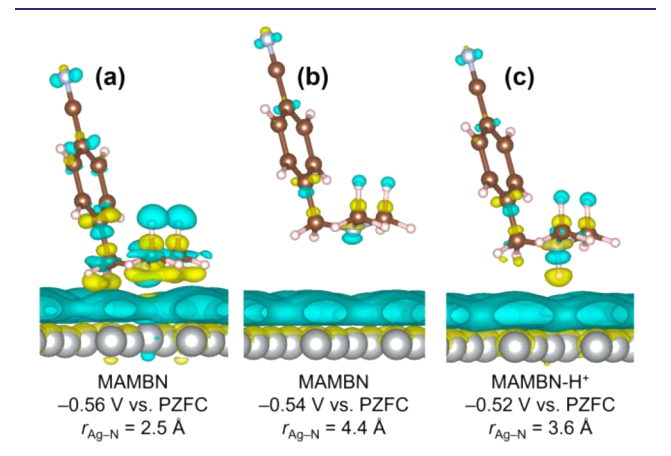


Figure 5. Interactions between Ag(100) and either product MAMBN or reactant MAMBN-H $^+$ molecules. (a,b) Product MAMBN (a) chemisorbed to and (b) physisorbed near Ag(100). (c) MAMBN-H $^+$ physisorbed near Ag(100). Charge density difference isosurfaces are shown with respect to the electrode PZFC, where the cyan and yellow indicate increases and decreases in electron density, respectively; the isosurface level is $0.00025 \text{ e}^-/\text{Bohr}^3$. Ag atoms are gray, N atoms are light blue, C atoms are brown, and H atoms are light pink. Further details are provided in the SI.

these molecules near the Ag(100) surface. These calculations employed a 4×4 unit cell, corresponding to a coverage of 0.72 molecules nm⁻². We performed similar analyses on closepacked Ag(111) and stepped Ag (322) surfaces. Further details are provided in the SI, Figures S2–S4.

On Ag(100), we identified a local minimum for chemisorption of MAMBN at a Ag-N distance of $r_{\rm Ag-N} \approx$ 2.5 Å (Figure 5a). This distance is consistent with previously calculated bond lengths of amines on Ag surfaces. 59,60 The presence of a covalent Ag-N bond in this configuration is further supported by the charge transfer between Ag(100) and the amine, as indicated by the charge density difference relative to the potential of zero free charge (PZFC) (Figure 5a). A covalent bond is also supported by the observed population of Ag-N bonding orbitals below the Fermi level, as determined from crystal orbital Hamilton population analysis (SI, Figure S5). The adsorption energies for chemisorbed MAMBN are calculated at PZFC using an uncharged unit cell. The adsorption energy of -0.79 eV suggests that the bond formed between MAMBN and Ag(100) is energetically favorable. The adsorption energy was insensitive to higher MAMBN coverage with a computed adsorption energy of -0.77 eV using a 3×3

We find that MAMBN adsorption is moderately stronger on Ag(322) steps ($\Delta E_{\rm ads} = -0.98$ eV, Figure S6). This trend aligns with the decreased bond order of Ag atoms on steps. We also find that MAMBN can interact with Ag(100) through π interactions between the benzonitrile and the surface at a distance of ~3.3 Å (SI, Figure S4). However, this structure does not correspond to the product directly after proton transfer from MAMBN-H⁺.

The MAMBN-H⁺ reactant must be oriented in a similar manner as depicted in Figure 5 to transfer its proton to the Ag electrode. In contrast to MAMBN, the MAMBN-H⁺ reactant does not chemisorb to the surface, as indicated by a chemical bonding analysis (Figure S7). This lack of chemisorption is attributed to the lack of a lone pair on the fully coordinated sp³ nitrogen. These calculations point to the likelihood that, following desolvation of the reactant MAMBN-H⁺ and product formation at -0.4 V vs Ag/AgCl (see Figure 3), the product MAMBN may be directly interacting by chemisorption with the electrode surface.

The next piece of evidence for the assignment of the 2200 cm⁻¹ peak to adsorbed MAMBN on the surface comes from a control experiment, where only the deprotonated MAMBN was subjected to the spectroelectrochemical study. The results are shown in Figure 6. Since this experiment is carried out in

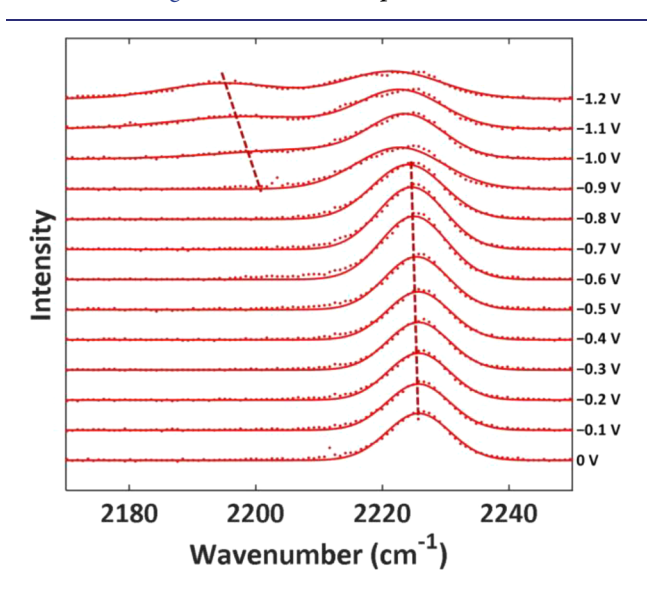


Figure 6. Potential dependent nitrile peak in a control experiment, where only the product MAMBN was present. The peak around 2227 cm⁻¹ does not Stark shift over a very large range of potential, indicating that the neutral MAMBN is not drawn into the EDL easily. It is not until a relatively high negative potential of ~ -1.0 V that a second Stark-shifting peak corresponding to the adsorbed MAMBN is observed. This peak appears at a much less negative potential when MAMBN is not drawn from the solution, but rather is produced by the Volmer reaction from MAMBN-H⁺, as seen in Figure 3.

the absence of protons, the Volmer reaction is not possible, and thus the peaks for the solvated MAMBN are observed until the potential is biased more negative than -1.0 V vs Ag/ AgCl. This observation indicates that unlike the positively charged MAMBN-H+ molecules, which are more electrostatically attracted to a negatively charged electrode, these molecules remain outside the EDL up to a much more negative potential. Below -1.0 V, the Stark shifting 2200 cm⁻¹ peak, which was also seen in the Volmer reaction in Figure 3, begins to appear. This observation suggests that MAMBN can be drawn from the solution and adsorbed on the silver electrode. In the case of the electrochemical Volmer reaction, however, the charged MAMBN-H⁺ is first drawn to the surface, and the deprotonated product is readily generated near the surface and available for adsorption. Based on the experimental and computational evidence discussed above, we can confidently assign the 2200 cm⁻¹ peak to the chemisorbed MAMBN product on the surface.

Figures 3 and 4 show that the product peak appears at around -0.4 V, less negative than the onset potential for the sustained steady state electrochemical current at -0.7 V. The explanation for this observation is revealed by spectroscopy and otherwise would remain hidden with electrochemical measurements alone. The appearance of the product peaks at less negative potentials than the onset for steady state current indicates that soon after entry into the EDL, PCET from some reactant MAMBN-H⁺ molecules has started to occur, turning over to the product MAMBN. This results in an adsorbed population of products on the surface. However, this population is stationary and does not turn over to yield a sustained electrochemical current. The net current due to a single layer of such population on the electrode surface is too small to be observable electrochemically at slow scan rates and can go undetected. However, spectroscopic observation of the surface reveals a buildup of this stationary population prior to the onset and sheds light on this otherwise hidden reaction. The spectroscopic signature of the new species observed between -0.4 and -0.7 V is consistent with a deprotonated molecule. Furthermore, the DMSO solvent is unlikely to be protonated, and the underpotential deposition (UPD) of hydrogen atoms on metals is well-known.⁴⁴ Thus, the most likely scenario is that the proton is adsorbed on the surface as a hydrogen atom after PCET from the donor molecule. Interestingly, this peak slightly diminishes in intensity after the onset potential, indicating that fewer MAMBN molecules are built up near the surface once the reaction turns over and is generating steady state current. In that scenario, fresh positively charged reactants are continuously brought to the negatively charged surface, displacing the adsorbed products built up near the electrode surface.

It is important to understand whether the -0.4 V potential at which products begin to appear spectroscopically is above or below the thermodynamic equilibrium potential E° for the reaction. Appearance of a monolayer or a few layers of product prior to the equilibrium potential is known as underpotential deposition in electrochemistry and is very well studied.⁴⁴ To identify the E° of the reaction, we conducted a series of open circuit potential measurements on a related amine (see SI)⁶³ and determined that E° is near -0.06 V vs Ag/AgCl, which is far from the -0.4 V value. Therefore, our observation of the products at -0.4 V is not due to UPD. The deposition occurs at more negative potentials than E° , but less negative than the steady current threshold. We conjecture that such subthreshold deposition may be more common than currently known because its electrochemical signature or current is rather small and easy to miss, especially at slow scan speeds. The above analysis shows that the potential for desolvation and formation of the stationary layer can be a significant fraction of the overpotential of the reaction. We hope that our study can inspire spectroscopic searching for adsorbed reaction products prior to current onset in a larger range of reactions to test the generality of this proposal.

Current Onset and Continued Stark shift of the Reactants and Products (-0.7 to -1.2 V). Finally, we will discuss the Stark shift of both the products and reactants starting from -0.4 V and continuing all the way to the end of our scan at -1.2 V. A potential of -0.7 V corresponds to the onset of steady state current corresponding to hydrogen evolution, as shown in Figures 3 and 4. A significant Stark shift is observed for both reactant MAMBN-H⁺ and product MAMBN, indicating that both reside within the EDL and

therefore are influenced by the electrode. Interestingly, the amount of shift per unit potential is not dramatically different between the reactant and the product, with MAMBN exhibiting a slightly larger Stark shift compared to MAMBN-H $^+$ (14 cm $^{-1}$ versus 10 cm $^{-1}$ over the potential range of -0.4 to -1.0 V).

The comparable sensitivity of the nitrile frequency to applied potential for MAMBN-H⁺ and MAMBN can be explained with input from our computational work. The isosurfaces in Figure 5 show that, upon a potential bias negative of PZFC, the charge density differences across the benzene ring and the nitrile are qualitatively similar between MAMBN-H⁺ and both the chemisorbed and physisorbed MAMBN. Bader analysis^{64–66} indicates minimal charge transfer from the electrode to the MAMBN or MAMBN-H⁺ (see SI, Figure S9). These analyses suggest that the nitrile frequency of MAMBN-H⁺ will respond similarly to that of chemisorbed and physisorbed MAMBN with applied potential. The small differences in these responses are most likely due to differences in the polarizability of the benzene ring.

Although MAMBN-H⁺ and MAMBN exhibit similar Stark behavior, the small difference between them that is observed experimentally is also supported by computations, as presented in Figure 7. A possible reason for the slightly larger shift for

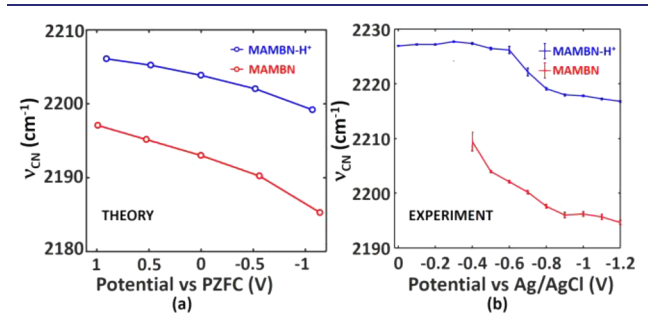


Figure 7. Frequency shifts of the reactant and the product from theory (left panel) (corresponding to the geometries in Figure 5a and 5c) and from experiment (right panel). The reactant frequency shifts are plotted in blue, and the product frequency shifts are plotted in red. The range of potentials in the experimental work is narrower due to the stability of the electrode. The slopes of the middle regions of the experimental curves are qualitatively similar to the slopes of the calculated curves. Note that the calculated frequencies at the most negative potentials are less reliable because of charge transfer from the electrode to the molecule (Figure S8) and likely proton transfer from MAMBN-H⁺.

MAMBN is that it can approach the electrode more closely and chemisorb, as shown in Figure 5. In contrast, MAMBN-H⁺ cannot chemisorb to the surface. Comparison of the vibrational shifts for MAMBN at two different distances from the electrode (Figure S8) shows that the Stark shift is greater when the molecule is closer to the electrode, as expected based on the significance of the polarizable benzene ring. We also calculate a Stark shift for a configuration where MAMBN interacts with Ag through π interactions because the charged electrode can polarize charge within the benzonitrile (Figure S4).

Our spectra show that the product MAMBN molecules adsorb on the surface after the reaction with an adequately long residence time to create a spectroscopically observable steady state population. Of course, this population is continuously exchanged for fresh reactant MAMBN-H⁺ to

maintain steady state current. The adsorbed population consumes some surface area of the electrode and affects the apparent kinetics of the reaction. Our spectroscopic evidence for such product accumulation near the surface will help inform and augment existing electrochemical kinetic models for this reaction.

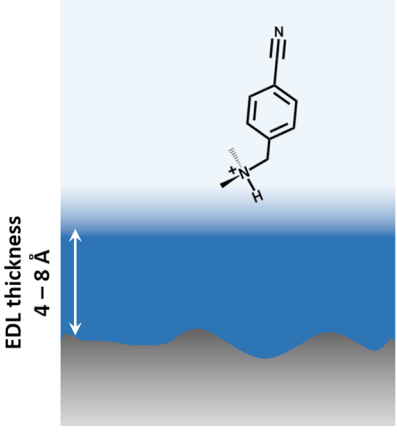
Since adsorbed MAMBN will occupy some electrode surface area, it will reduce the availability of surface sites for PCET and impede the reaction. Adsorption and desorption of the reactant and product, respectively, can be tuned by the choice of the donor molecule, the solvent, or the electrode. In aqueous hydrogen evolution, for example, adsorption of deprotonated donor molecules can either promote or limit reaction rates.⁶⁷

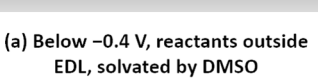
The reverse scan provides information about whether the product MAMBN is permanently adsorbed on the electrode surface. While running the reverse scan from -1.2 to 0 V, both the reactant MAMBN-H+ and the product MAMBN peaks backtrack their frequency shifts, until the MAMBN peak disappears, and only the MAMBN-H+ peak remains without any Stark shift. This observation indicates that the product reversibly adsorbs and desorbs to the electrode, and that the conversion between reactants and products is consistent between forward and reverse scans, with no detectable formation of side products. It is also noteworthy that in the reverse scan a significant amount of the product that was produced at more negative potentials remains visible even after the current no longer flows, indicating that subthreshold interaction between the products and the electrode surface discussed earlier is perhaps a function of the potential and not the direction of the scan.

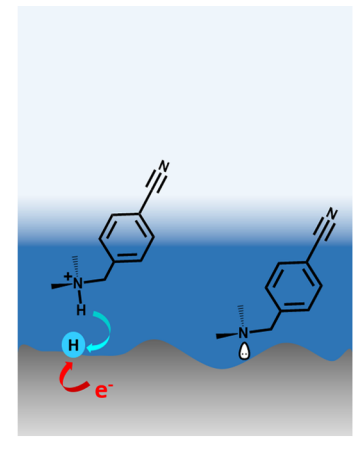
Finally, we comment on the variation of spectral line widths as a function of potential. As seen in Figure 3, we observe differences in line width in the spectra of reactants residing outside the EDL and the chemisorbed products. Such differences may arise from variation of the electrostatic environments for the two cases. Line width variation as a function of applied potential was previously observed by us for covalently bound benzonitriles as a function of potential.³⁷ Given that previous literature has identified intramolecular sources of damping for the nitrile vibration, ⁶⁸ however, we caution against an interpretation of line widths as solely arising from the electrostatic variations.

CONCLUSIONS

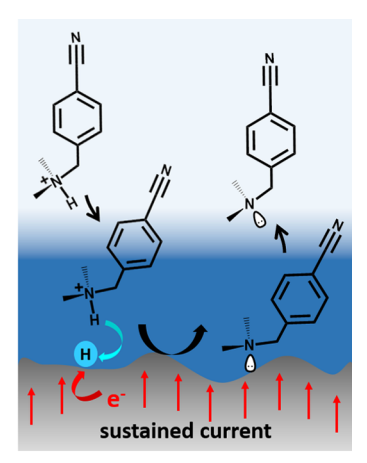
A summary of the Volmer reaction based on insights from the spectroelectrochemical experiments and theoretical calculations is presented in Figure 8. From our joint experimental and theoretical analysis, we have categorized three main stages for the progression of the reaction as a function of applied potential. These interpretations were facilitated by an understanding that molecular species positioned within the EDL will Stark shift with applied potential, while those outside of the EDL will not. First, the reactant MAMBN-H+ molecules remain solvated outside of the EDL prior to the desolvation potential of -0.4 V vs Ag/AgCl (Figure 8a). Next, after the molecule enters the EDL, the interfacial Volmer reaction leads to the formation of a stationary population of products (Figure 8b). Finally, at potentials negative of -0.7 V vs Ag/AgCl, the negatively charged surface attracts additional reactant MAMBN-H⁺ molecules, displacing the stationary MAMBN molecules near the electrode surface and enabling the onset of steady state current (Figure 8c).







(b) Between -0.4 V and -0.7 V, range for formation of stationary product



(c) More negative than -0.7 V, sustained current

Figure 8. Schematic figure showing the sequence of events for the reaction based on our experimental and computational data. (a) Below -0.4 V, the reactant MAMBN-H⁺ molecules, which are solvated by DMSO, reside outside the EDL and do not feel the polarizing influence of the electrode and therefore do not exhibit a Stark shift. (b) Within the potential range of -0.4 V to -0.7 V, the reactant molecules partially shed their bulk solvation shell and enter the EDL, as evidenced by their Stark shift. Some of the reactant MAMBN-H⁺ molecules undergo the Volmer reaction and form MAMBN, as evidenced by the largely red-shifted peak in our data. Lack of electrochemical current in this range suggests that this is a stationary population and does not turn over. Computational and experimental observations suggest that MAMBN is chemisorbed on the surface. (c) At potentials more negative of -0.7 V, the reaction can turn over yielding a steady state current. Correspondingly, a steady state population of MAMBN-H⁺ and MAMBN that continue to Stark shift with potential is observed.

By combining a Stark shift vibrational probe with a proton donor, we have revealed several features of the Volmer reaction through operando vibrational spectroscopy that were not accessible from electrochemical measurements alone. We anticipate that many of the concepts elucidated by this work are general and applicable to a wide range of electrochemical reactions. Specifically, formation of a stationary layer of products prior to the onset of steady state current is quite likely to occur for other reactions. However, its detection by conventional electrochemical methods, especially in slow scans, may not be possible. Surface sensitive spectroscopic probes, such as the one used here, can reveal such hidden processes. A significant focus in electrochemistry is understanding the onset of reactions and the processes controlling overpotentials. Our finding of separate onsets for the formation of a stationary layer of products and the attainment of steady current may inspire electrochemists and surface scientists to further explore and exploit such concepts.

Our work inspires the following design principles for further understanding and optimizing interfacial PCET reactions, where the goal is to favor adsorption of the reactant and desorption of the product. For example, the double layer may be optimized by the choice of tailored surfactants to facilitate entry and alignment of the proton donors during the reaction. In addition, the interface could be designed to ensure that the discharged carrier does not adsorb on the surface but instead is solvated by the surfactant.

While these experiments were performed on silver electrodes, we believe that several of the results presented here are generalizable to other metallic electrodes. The adsorption of products on the electrode surface will vary for different electrodes and proton donors. Understanding the relationships between different electrode-donor combinations and PCET reaction mechanisms is an important topic for further study. Moreover, rational design strategies to tailor the desolvation threshold of proton donors may be developed by tuning the

properties of the solvent and electrolyte, as well as the PZFC of the electrode, to impact the electrostatics of the EDL. We conjecture that an analogous desolvation threshold may exist for the hydronium ion, although further work is needed to measure and model such systems. This study highlights the insights that can be gained by attaching well-defined vibrational probes to electrochemical reactants or catalysts.

ASSOCIATED CONTENT

Supporting Information

The Supporting Information is available free of charge at https://pubs.acs.org/doi/10.1021/jacs.1c01977.

Details of computational methods and measurement of the equilibrium potential for the triethylamine-triethylammonium redox couple (PDF)

AUTHOR INFORMATION

Corresponding Author

Jahan M. Dawlaty — Department of Chemistry, University of Southern California, Los Angeles, California 90089, United States; orcid.org/0000-0001-5218-847X; Phone: 213-740-9337; Email: dawlaty@usc.edu

Authors

Sohini Sarkar — Department of Chemistry, University of Southern California, Los Angeles, California 90089, United States; orcid.org/0000-0002-5714-6778

Anwesha Maitra – Department of Chemistry, University of Southern California, Los Angeles, California 90089, United States

William R. Lake — Department of Chemistry, Yale University, New Haven, Connecticut 06520, United States; orcid.org/0000-0001-8182-3583

Robert E. Warburton — Department of Chemistry, Yale University, New Haven, Connecticut 06520, United States; orcid.org/0000-0002-9693-307X

Sharon Hammes-Schiffer — Department of Chemistry, Yale University, New Haven, Connecticut 06520, United States; orcid.org/0000-0002-3782-6995

Complete contact information is available at: https://pubs.acs.org/10.1021/jacs.1c01977

Notes

The authors declare no competing financial interest.

ACKNOWLEDGMENTS

The authors acknowledge support from several sources. This work was supported by the Air Force Office of Scientific Research under AFOSR Award FA9550-18-1-0420. S.S. was also partially supported by the Research Corporation for Science Advancement (RCSA) through their Cottrell Fellowship for ensuring continuity of funding for postdoctoral scholars under Award 27445, and cosponsored by the National Science Foundation under Award CHE-2039044. S.H.S. was also partially supported by Air Force Office of Scientific Research under AFOSR Award FA9550-18-1-0134.

REFERENCES

- (1) Santos, E.; Hindelang, P.; Quaino, P.; Schulz, E. N.; Soldano, G.; Schmickler, W. Hydrogen Electrocatalysis on Single Crystals and on Nanostructured Electrodes. *ChemPhysChem* **2011**, *12*, 2274–2279.
- (2) Hammes-Schiffer, S. Theory of Proton-Coupled Electron Transfer in Energy Conversion Processes. *Acc. Chem. Res.* **2009**, *42*, 1881–1889.
- (3) Hammes-Schiffer, S.; Soudackov, A. V. Proton-Coupled Electron Transfer in Solution, Proteins, and Electrochemistry. *J. Phys. Chem. B* **2008**, *112*, 14108–14123.
- (4) Weinberg, D. R.; Gagliardi, C. J.; Hull, J. F.; Murphy, C. F.; Kent, C. A.; Westlake, B. C.; Paul, A.; Ess, D. H.; McCafferty, D. G.; Meyer, T. J. Proton-Coupled Electron Transfer. *Chem. Rev.* **2012**, *112*, 4016–4093.
- (5) Warren, J. J.; Tronic, T. A.; Mayer, J. M. Thermochemistry of Proton-Coupled Electron Transfer Reagents and Its Implications. *Chem. Rev.* **2010**, *110*, 6961–7001.
- (6) Darcy, J. W.; Koronkiewicz, B.; Parada, G. A.; Mayer, J. M. A Continuum of Proton-Coupled Electron Transfer Reactivity. *Acc. Chem. Res.* **2018**, *51*, 2391–2399.
- (7) Meyer, T. J.; Huynh, M. H. V.; Thorp, H. H. The Possible Role of Proton-Coupled Electron Transfer (PCET) in Water Oxidation by Photosystem II. *Angew. Chem., Int. Ed.* **2007**, *46*, 5284–5304.
- (8) Costentin, C.; Robert, M.; Savéant, J.-M. Catalysis of the Electrochemical Reduction of Carbon Dioxide. *Chem. Soc. Rev.* **2013**, 42, 2423–2436.
- (9) Keith, J. A.; Grice, K. A.; Kubiak, C. P.; Carter, E. A. Elucidation of the Selectivity of Proton-Dependent Electrocatalytic CO₂ Reduction by Fac-Re(Bpy)(CO)₃Cl. *J. Am. Chem. Soc.* **2013**, *135*, 15823–15829.
- (10) Mondal, B.; Rana, A.; Sen, P.; Dey, A. Intermediates Involved in the 2e⁻/2H⁺ Reduction of CO₂ to CO by Iron(0) Porphyrin. *J. Am. Chem. Soc.* **2015**, *137*, 11214–11217.
- (11) Nocera, D. G. Chemistry of Personalized Solar Energy. *Inorg. Chem.* **2009**, 48, 10001–10017.
- (12) Jackson, M. N.; Surendranath, Y. Donor-Dependent Kinetics of Interfacial Proton-Coupled Electron Transfer. *J. Am. Chem. Soc.* **2016**, 138, 3228–3234.
- (13) Goldsmith, Z. K.; Lam, Y. C.; Soudackov, A. V.; Hammes-Schiffer, S. Proton Discharge on a Gold Electrode from Triethylammonium in Acetonitrile: Theoretical Modeling of Potential-Dependent Kinetic Isotope Effects. *J. Am. Chem. Soc.* **2019**, *141*, 1084–1090.
- (14) Warburton, R. E.; Hutchison, P.; Jackson, M. N.; Pegis, M. L.; Surendranath, Y.; Hammes-Schiffer, S. Interfacial Field-Driven

- Proton-Coupled Electron Transfer at Graphite-Conjugated Organic Acids. J. Am. Chem. Soc. 2020, 142, 20855–20864.
- (15) Mathew, R.; Kayal, S.; Yapamanu, A. L. Excited State Structural Dynamics of 4-Cyano-4'-Hydroxystilbene: Deciphering the Signatures of Proton-Coupled Electron Transfer Using Ultrafast Raman Loss Spectroscopy. *Phys. Chem. Chem. Phys.* **2019**, *21*, 22409–22419.
- (16) Frydendal, R.; Seitz, L. C.; Sokaras, D.; Weng, T.-C.; Nordlund, D.; Chorkendorff, I.; Stephens, I. E. L.; Jaramillo, T. F. Operando Investigation of Au-MnO_x Thin Films with Improved Activity for the Oxygen Evolution Reaction. *Electrochim. Acta* **2017**, 230, 22–28.
- (17) Waegele, M. M.; Culik, R. M.; Gai, F. Site-Specific Spectroscopic Reporters of the Local Electric Field, Hydration, Structure, and Dynamics of Biomolecules. *J. Phys. Chem. Lett.* **2011**, 2, 2598–2609.
- (18) Gunathunge, C. M.; Li, J.; Li, X.; Waegele, M. M. Surface-Adsorbed Co as an Infrared Probe of Electrocatalytic Interfaces. *ACS Catal.* **2020**, *10*, 11700–11711.
- (19) Ge, A.; Videla, P. E.; Lee, G. L.; Rudshteyn, B.; Song, J.; Kubiak, C. P.; Batista, V. S.; Lian, T. Interfacial Structure and Electric Field Probed by in Situ Electrochemical Vibrational Stark Effect Spectroscopy and Computational Modeling. *J. Phys. Chem. C* **2017**, *121*, 18674–18682.
- (20) Fried, S. D.; Boxer, S. G. Measuring Electric Fields and Noncovalent Interactions Using the Vibrational Stark Effect. *Acc. Chem. Res.* **2015**, *48*, 998–1006.
- (21) Baldelli, S. Probing Electric Fields at the Ionic Liquid-Electrode Interface Using Sum Frequency Generation Spectroscopy and Electrochemistry. *J. Phys. Chem. B* **2005**, *109*, 13049–13051.
- (22) Schultz, Z. D.; Shaw, S. K.; Gewirth, A. A. Potential Dependent Organization of Water at the Electrified Metal-Liquid Interface. *J. Am. Chem. Soc.* **2005**, *127*, 15916–15922.
- (23) Shaw, S. K.; Lagutchev, A.; Dlott, D. D.; Gewirth, A. A. Electrochemically Driven Reorientation of Three Ionic States of P-Aminobenzoic Acid on Ag(111). *J. Phys. Chem. C* **2009**, *113*, 2417–2424.
- (24) Heidary, N.; Ly, K. H.; Kornienko, N. Probing Co2 Conversion Chemistry on Nanostructured Surfaces with Operando Vibrational Spectroscopy. *Nano Lett.* **2019**, *19*, 4817–4826.
- (25) Kornienko, N.; Ly, K. H.; Robinson, W. E.; Heidary, N.; Zhang, J. Z.; Reisner, E. Advancing Techniques for Investigating the Enzyme-Electrode Interface. *Acc. Chem. Res.* **2019**, *52*, 1439–1448.
- (26) Waegele, M. M.; Gunathunge, C. M.; Li, J.; Li, X. How Cations Affect the Electric Double Layer and the Rates and Selectivity of Electrocatalytic Processes. *J. Chem. Phys.* **2019**, *151*, 160902.
- (27) Gunathunge, C. M.; Li, J.; Li, X.; Hong, J. J.; Waegele, M. M. Revealing the Predominant Surface Facets of Rough Cu Electrodes under Electrochemical Conditions. *ACS Catal.* **2020**, *10*, 6908–6923.
- (28) Shaw, S. K.; Berná, A.; Feliu, J. M.; Nichols, R. J.; Jacob, T.; Schiffrin, D. J. Role of Axially Coordinated Surface Sites for Electrochemically Controlled Carbon Monoxide Adsorption on Single Crystal Copper Electrodes. *Phys. Chem. Chem. Phys.* **2011**, *13*, 5242–5251.
- (29) Rey, N. G.; Dlott, D. D. Studies of Electrochemical Interfaces by Broadband Sum Frequency Generation. *J. Electroanal. Chem.* **2017**, 800, 114–125.
- (30) Fried, S. D.; Bagchi, S.; Boxer, S. G. Extreme Electric Fields Power Catalysis in the Active Site of Ketosteroid Isomerase. *Science* **2014**, *346*, 1510.
- (31) Fried, S. D.; Boxer, S. G. Electric Fields and Enzyme Catalysis. *Annu. Rev. Biochem.* **2017**, *86*, 387–415.
- (32) Hammes-Schiffer, S. Catalytic Efficiency of Enzymes: A Theoretical Analysis. *Biochemistry* **2013**, *52*, 2012–2020.
- (33) Slocum, J. D.; Webb, L. J. Measuring Electric Fields in Biological Matter Using the Vibrational Stark Effect of Nitrile Probes. *Annu. Rev. Phys. Chem.* **2018**, *69*, 253–271.
- (34) Sorenson, S. A.; Patrow, J. G.; Dawlaty, J. M. Solvation Reaction Field at the Interface Measured by Vibrational Sum Frequency Generation Spectroscopy. *J. Am. Chem. Soc.* **2017**, *139*, 2369–2378.

- (35) Patrow, J. G.; Sorenson, S. A.; Dawlaty, J. M. Direct Spectroscopic Measurement of Interfacial Electric Fields near an Electrode under Polarizing or Current-Carrying Conditions. *J. Phys. Chem. C* 2017, 121, 11585–11592.
- (36) Sarkar, S.; Maitra, A.; Banerjee, S.; Thoi, V. S.; Dawlaty, J. M. Electric Fields at Metal-Surfactant Interfaces: A Combined Vibrational Spectroscopy and Capacitance Study. *J. Phys. Chem. B* **2020**, *124*, 1311–1321.
- (37) Sarkar, S.; Patrow, J. G.; Voegtle, M. J.; Pennathur, A. K.; Dawlaty, J. M. Electrodes as Polarizing Functional Groups: Correlation between Hammett Parameters and Electrochemical Polarization. *J. Phys. Chem. C* **2019**, *123*, 4926–4937.
- (38) Pennathur, A. K.; Voegtle, M. J.; Menachekanian, S.; Dawlaty, J. M. Strong Propensity of Ionic Liquids in Their Aqueous Solutions for an Organic-Modified Metal Surface. *J. Phys. Chem. B* **2020**, *124*, 7500–7507.
- (39) Voegtle, M. J.; Pal, T.; Pennathur, A. K.; Menachekanian, S.; Patrow, J. G.; Sarkar, S.; Cui, Q.; Dawlaty, J. M. Interfacial Polarization and Ionic Structure at the Ionic Liquid-Metal Interface Studied by Vibrational Spectroscopy and Molecular Dynamics Simulations. *J. Phys. Chem. B* **2021**, *125*, 2741–2753.
- (40) Goldsmith, Z. K.; Secor, M.; Hammes-Schiffer, S. Inhomogeneity of Interfacial Electric Fields at Vibrational Probes on Electrode Surfaces. ACS Cent. Sci. 2020, 6, 304–311.
- (41) Lapidus, S. H.; Rajput, N. N.; Qu, X.; Chapman, K. W.; Persson, K. A.; Chupas, P. J. Solvation Structure and Energetics of Electrolytes for Multivalent Energy Storage. *Phys. Chem. Chem. Phys.* **2014**, *16*, 21941–21945.
- (42) Banerjee, S.; Han, X.; Thoi, V. S. Modulating the Electrode-Electrolyte Interface with Cationic Surfactants in Carbon Dioxide Reduction. *ACS Catal.* **2019**, *9*, 5631–5637.
- (43) Guo, C.; Ran, J.; Vasileff, A.; Qiao, S.-Z. Rational Design of Electrocatalysts and Photo(Electro)Catalysts for Nitrogen Reduction to Ammonia (NH₃) under Ambient Conditions. *Energy Environ. Sci.* **2018**, *11*, 45–56.
- (44) Herrero, E.; Buller, L. J.; Abruña, H. D. Underpotential Deposition at Single Crystal Surfaces of Au, Pt, Ag and Other Materials. *Chem. Rev.* **2001**, *101*, 1897–1930.
- (45) Schouten, K. J. P.; van der Niet, M. J. T. C.; Koper, M. T. M. Impedance Spectroscopy of H and OH Adsorption on Stepped Single-Crystal Platinum Electrodes in Alkaline and Acidic Media. *Phys. Chem. Chem. Phys.* **2010**, *12*, 15217–15224.
- (46) Sharma, B.; Frontiera, R. R.; Henry, A.-I.; Ringe, E.; Van Duyne, R. P. Sers: Materials, Applications, and the Future. *Mater. Today* **2012**, *15*, 16–25.
- (47) Grimme, S.; Antony, J.; Ehrlich, S.; Krieg, H. A Consistent and Accurate Ab Initio Parametrization of Density Functional Dispersion Correction (DFT-D) for the 94 Elements H-Pu. *J. Chem. Phys.* **2010**, 132, 154104.
- (48) Giannozzi, P.; et al. Quantum Espresso: A Modular and Open-Source Software Project for Quantum Simulations of Materials. *J. Phys.: Condens. Matter* **2009**, 21, 395502.
- (49) Giannozzi, P.; et al. Advanced Capabilities for Materials Modelling with Quantum Espresso. *J. Phys.: Condens. Matter* **2017**, 29, 465901.
- (50) Perdew, J. P.; Burke, K.; Ernzerhof, M. Generalized Gradient Approximation Made Simple. *Phys. Rev. Lett.* **1996**, *77*, 3865–3868.
- (51) Andreussi, O.; Dabo, I.; Marzari, N. Revised Self-Consistent Continuum Solvation in Electronic-Structure Calculations. *J. Chem. Phys.* **2012**, *136*, 064102.
- (52) Lu, Z.; Manias, E.; Macdonald, D. D.; Lanagan, M. Dielectric Relaxation in Dimethyl Sulfoxide/Water Mixtures Studied by Microwave Dielectric Relaxation Spectroscopy. *J. Phys. Chem. A* **2009**, *113*, 12207–12214.
- (53) Kastlunger, G.; Lindgren, P.; Peterson, A. A. Controlled-Potential Simulation of Elementary Electrochemical Reactions: Proton Discharge on Metal Surfaces. *J. Phys. Chem. C* **2018**, *122*, 12771–12781.

- (54) Ge, A.; Kastlunger, G.; Meng, J.; Lindgren, P.; Song, J.; Liu, Q.; Zaslavsky, A.; Lian, T.; Peterson, A. A. On the Coupling of Electron Transfer to Proton Transfer at Electrified Interfaces. *J. Am. Chem. Soc.* **2020**, *142*, 11829–11834.
- (55) Schkolnik, G.; Salewski, J.; Millo, D.; Zebger, I.; Franzen, S.; Hildebrandt, P. Vibrational Stark Effect of the Electric-Field Reporter 4-Mercaptobenzonitrile as a Tool for Investigating Electrostatics at Electrode/SAM/Solution Interfaces. *Int. J. Mol. Sci.* **2012**, *13*, 7466–7482.
- (56) Kovacs, G. J.; Loutfy, R. O.; Vincett, P. S.; Jennings, C.; Aroca, R. Distance Dependence of Sers Enhancement Factor from Langmuir-Blodgett Monolayers on Metal Island Films: Evidence for the Electromagnetic Mechanism. *Langmuir* **1986**, *2*, 689–694.
- (57) Allen, J. B.; Larry, R. F. Electrochemical Methods Fundamentals and Applications; John Wiley & Sons: 2001.
- (58) Chmiola, J.; Largeot, C.; Taberna, P.-L.; Simon, P.; Gogotsi, Y. Desolvation of Ions in Subnanometer Pores and Its Effect on Capacitance and Double-Layer Theory. *Angew. Chem., Int. Ed.* **2008**, 47, 3392–3395.
- (59) Stachiotti, M. G. First-Principles Study of the Adsorption of NH₃ on Ag Surfaces. *Phys. Rev. B: Condens. Matter Mater. Phys.* **2009**, 79, 115405.
- (60) Martínez, A. Bonding Interactions of Metal Clusters [Mn (M= Cu, Ag, Au; N = 1-4)] with Ammonia. Are the Metal Clusters Adequate as a Model of Surfaces? *J. Braz. Chem. Soc.* **2005**, *16*, 337–344
- (61) Abild-Pedersen, F.; Greeley, J.; Studt, F.; Rossmeisl, J.; Munter, T. R.; Moses, P. G.; Skúlason, E.; Bligaard, T.; Nørskov, J. K. Scaling Properties of Adsorption Energies for Hydrogen-Containing Molecules on Transition-Metal Surfaces. *Phys. Rev. Lett.* **2007**, *99*, 016105.
- (62) Calle-Vallejo, F.; Loffreda, D.; Koper, M. T. M.; Sautet, P. Introducing Structural Sensitivity into Adsorption-Energy Scaling Relations by Means of Coordination Numbers. *Nat. Chem.* **2015**, *7*, 403–410.
- (63) Wise, C. F.; Agarwal, R. G.; Mayer, J. M. Determining Proton-Coupled Standard Potentials and X-H Bond Dissociation Free Energies in Nonaqueous Solvents Using Open-Circuit Potential Measurements. J. Am. Chem. Soc. 2020, 142, 10681–10691.
- (64) Tang, W.; Sanville, E.; Henkelman, G. A Grid-Based Bader Analysis Algorithm without Lattice Bias. *J. Phys.: Condens. Matter* **2009**, *21*, 084204.
- (65) Sanville, E.; Kenny, S. D.; Smith, R.; Henkelman, G. Improved Grid-Based Algorithm for Bader Charge Allocation. *J. Comput. Chem.* **2007**, 28, 899–908.
- (66) Henkelman, G.; Arnaldsson, A.; Jónsson, H. A Fast and Robust Algorithm for Bader Decomposition of Charge Density. *Comput. Mater. Sci.* **2006**, *36*, 354–360.
- (67) McCrum, I. T.; Koper, M. T. M. The Role of Adsorbed Hydroxide in Hydrogen Evolution Reaction Kinetics on Modified Platinum. *Nat. Energy* **2020**, *5*, 891–899.
- (68) Pandey, H. D.; Leitner, D. M. Vibrational States and Nitrile Lifetimes of Cyanophenylalanine Isotopomers in Solution. *J. Phys. Chem. A* **2018**, 122, 6856–6863.